# Flexible well patterns and cashflow optimisation on large-scale geothermal field development

Kane, Entela; Leeuwenburgh, Olwijn; Joosten, Gerard; Daniilidis, Alexandros; Bruhn, David

**DOI**
10.1016/j.renene.2025.122494

**Publication date**
2025

**Document Version**
Final published version

**Published in**
Renewable Energy

Renewable Energy 243 (2025) 122494

Contents lists available at ScienceDirect

Renewable Energy

journal homepage: www.elsevier.com/locate/renene

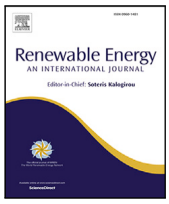

# Flexible well patterns and cashflow optimisation on large-scale geothermal field development

Entela Kane [a,*], Olwijn Leeuwenburgh [b], Gerard Joosten [c], Alexandros Daniilidis [a], David Bruhn [a,d]

[a] Department of Geosciences and Engineering, Faculty of Civil Engineering and Geosciences, Delft University of Technology, Stevinweg 1, Delft, 2628 CN, South Holland, The Netherlands
[b] TNO, Princetonlaan 6, Utrecht, 3584 CB, Utrecht, The Netherlands
[c] Shell Global Solutions International B.V., Grasweg 39, Amsterdam, 1031 HW, North Holland, The Netherlands
[d] Competence Centre Global Georesources, Fraunhofer IEG, Germany

ARTICLE INFO

*Keywords:*
Flexible well patterns
Well density function
Large-scale geothermal field development
Cashflow
Optimisation

ABSTRACT

The Netherlands aims to be CO2 neutral by 2050, aligning with the Paris Agreement. To achieve this, it is crucial to increase the contribution of geothermal energy to renewable energy sources, necessitating large-scale exploitation to speed up the energy transition. Only small-scale (1–2 km) geothermal field developments exist in the Netherlands primarily for heating. Expanding to extensive geothermal fields (>10 km length) requires a strategic approach to well placement and consideration of the economic constraints associated with geothermal projects. The heterogeneity of the subsurface is a critical factor in developing large-scale geothermal reservoirs. This study introduces an innovative approach to optimising well placement based on geological trends, using a well-density function as a proof of concept. Implementing and optimising flexible well patterns for large-scale geothermal developments significantly enhances profitability compared to conventional oil and gas industry methods. Optimised flexible well patterns favour a long-term utilisation of energy recovered, minimise pressure extrema in the reservoir, and improve sweep efficiency. However, their application depends on reservoir operational decisions. The optimisation process ensures economic viability, even with lower heat prices. Broadly, this methodology could be key to scaling up geothermal developments to meet the objectives of the Paris Agreement.

## 1. Introduction

The Netherlands, among other countries, has set goals to increase the contribution of geothermal energy from 0.5% of the total national heat production to 5% by 2030 [1]. So far the contribution has been achieved through the deployment of small-scale geothermal projects using well doublets [2]. Several authors have suggested geothermal field development with repeated doublets to upscale geothermal operations [3–7]. Upscaling operations from individual well doublets to multiple wells increases the density of wells for a given reservoir unit, leading to an optimised use of the subsurface. Thus, a higher density of operations can lead to greater energy efficiency of the systems. Previous research suggested that an extension of doublets to well patterns used in oil and gas field development is necessary to upscale geothermal field developments [8]. Well patterns discussed in previous studies were usually derived from oil and gas development like line-drive and 5-spot [9,10].

One of the many purposes of well patterns developed for oil and gas was to improve economic constraints that partially stem from the heterogeneity of the subsurface, by tuning well spacing through injector-producer placement to those large-scale heterogeneities [11,12]. Roberts et al. [13] showcased the large-scale geological character of spatially heterogeneous geological formations, demonstrating a geological model with a large-scale linear trend observed in porosity or thickness. Willems et al. [14] discussed the large-scale reservoir nature of the West Netherlands Basin with a channel belt of 10 km. Moreover, several researchers [15,16] have discussed the large-scale heterogeneous nature of fluvial systems and the impact of heterogeneity on the cold front position. The heterogeneous character of geological formations motivates the adoption of a collective and coordinated approach, leading to the optimal recovery of heat.

There are several studies on the concept of optimisation of individual well locations in oil and gas field developments [9,12,17–20]. The concept of optimisation of individual well locations on small-scale geothermal fields has already been discussed for the Netherlands [5,6]. Several authors have captured the concept of optimisation of individual

* Corresponding author.
*E-mail address:* E.Kane@tudelft.nl (E. Kane).

https://doi.org/10.1016/j.renene.2025.122494
Received 3 September 2024; Received in revised form 20 January 2025; Accepted 22 January 2025
Available online 30 January 2025

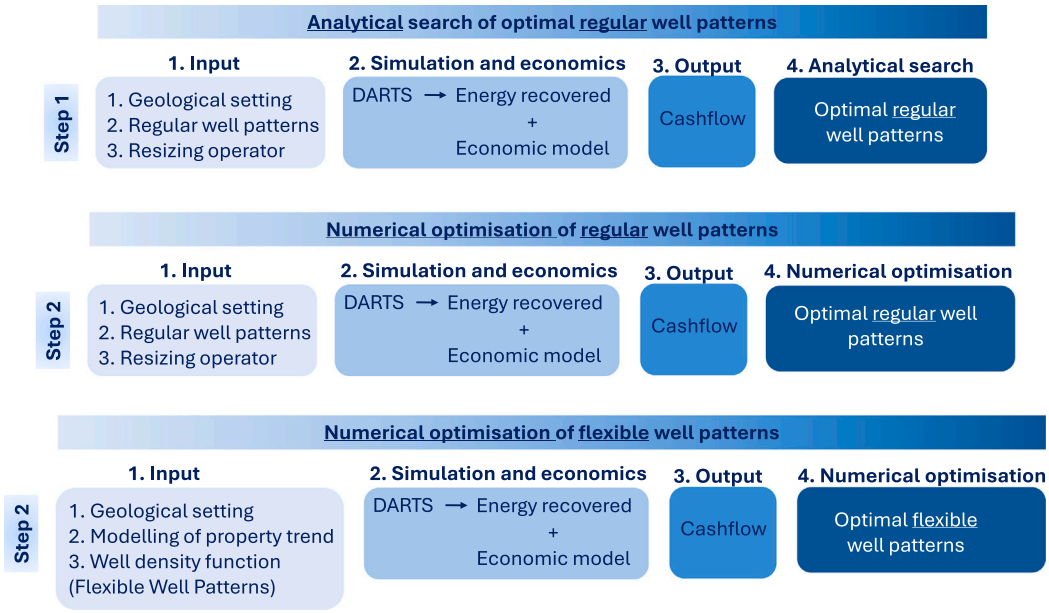


**Fig. 1.** Visual representation of the workflow adopted for the current research. The process includes three different optimisation routines on the same geological setting and the results will be compared in the end to infer the optimal development strategy.

geothermal well placement or doublets [21–23]. Olwunalu et al. [9,24] have extensively studied well pattern operators that distort the shape, size, orientation, type, and well locations. Zhang et al. [25] suggested a method of large-scale optimisation of geothermal fields; however, the methodology did not consider flexibility on well placement based on geological heterogeneities and did not include economic constraints.

The research above covers a rather localised approach in well placement rather than a collective approach. This study demonstrates the possibility and benefits of adapting and optimising well pattern parameters that control well density to reflect trends in geological properties. A literature gap exists in translating large-scale geological trends into a numerically optimised well placement problem. Furthermore, individual well location optimisation is a computationally challenging problem. Nasir et al. [26] proved that the number of optimisation variables scales with the maximum number of wells considered.

In this study, we attempt to close the abovementioned gap with a concept for large-scale geothermal field development to cover the heat demand in the Netherlands and beyond. We suggest a proof of concept of an innovative approach of flexible well patterns where we model well placement according to a large-scale trend of geological property. The applied methodology aims to reduce the number of optimised control variables in well placement, considering a trend in well placement or spacing across a defined direction. The optimisation targets economic factors as in previous studies [27,28].

## 2. Methodology

### 2.1. Workflow

We present the workflow we followed to infer the optimal development strategies for the tested geological scenarios. Fig. 1 demonstrates the steps of the process. The components of each step will be further analysed in the following sections. We adopted a 3-step strategy where each step targets to deliver the optimal development strategy for each geological setting with the assigned well pattern and optimisation strategy. At the end of the process, we compare the results of each well pattern and optimisation method to address the most profitable scenarios and further discuss the energy recovered.

### 2.2. Geothermal geological models

This chapter describes the different synthetic geological models we created to test the proposed field development approach. The necessity of large-scale heterogeneous geological models motivated the construction of synthetic models instead of using real case studies.

We considered two common types of heterogeneity encountered in the subsurface, namely large-scale trends ($10 * 10$ km) resulting for example from the presence of river systems and associated with channel features, as proof of concept. The synthetic geological models with different properties were described with a trend. These trends represented lithological variations of the geological formations such as a large-scale channel belt [14] and transitioning from shale to sand-dominated formations [13].

We created two models, one with a linear trend and one with a Gaussian trend in a chosen geological property, $p$. In this case, we modelled porosity. The geological model with a linear trend in porosity represents a transition from porous sandstones to a shally-dominating formation and has been discussed by [13]. The Gaussian trend describes a large-scale channel occurring from the sediments deposited in old river systems. All geological properties were adopted from geological settings in the Dutch subsurface [14,29]. The lower porosity corresponds to the lithology of shale and areas with higher porosity to sandstone.

The models are three-dimensional $(x, y, z)$. However, only two dimensions $(x, y)$ contributed to fluid and heat flow to establish that the 2-dimensional change of well location can lead to optimal heat recovery. The third dimension ($z$; thickness), only minimally contributes to flow compared to the other two directions to eliminate depth-dependent preferential pathways for fluid and heat flow, adding more complexity to the optimisation process. The z-dimension solely added a numerical volume to the numerical cells, which consisted of part of the simulation set-up. We modelled the porosity, permeability, bulk heat capacity, and bulk conductivity of the reservoir according to Eqs. (1), (2) for the linear and Gaussian geological models, respectively.

$$p = -ax + b \tag{1}$$

where $a = \frac{p_2 - p_1}{nx}$, $b = p_2$ and $nx$ is the reservoir length. $p_1$ and $p_2$ stand for the values of the properties we modelled: porosity, permeability,

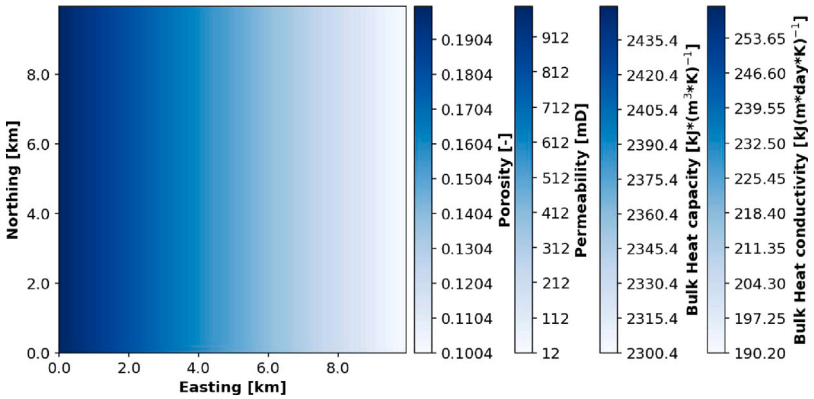


**Fig. 2.** Visual representation of porosity, permeability in x-y directions, bulk heat capacity, and bulk heat conductivity of the geological model with a linear trend in the $x$-direction.

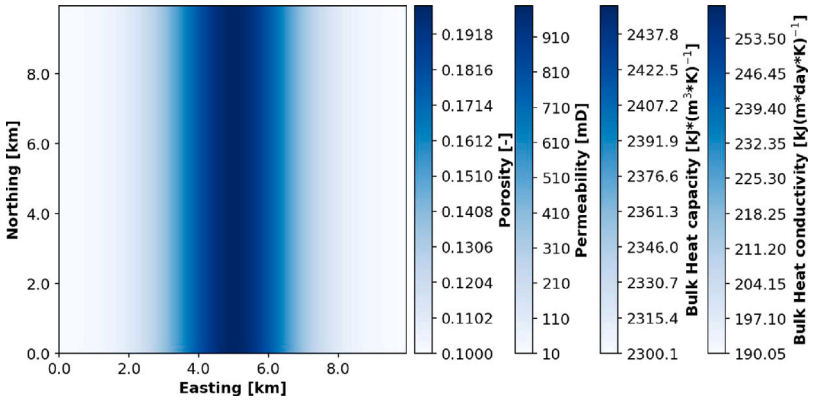


**Fig. 3.** Visual representation of porosity, permeability in x-y directions, bulk heat capacity, and bulk heat conductivity of the geological model with a Gaussian trend in the $x$-direction.

**Table 1**
Constant parameters used in geological modelling with a linear and Gaussian trend.

| Property (p) | Annotation | $p_1$ Value | $p_2$ Value | Untits (SI) |
|---|---|---|---|---|
| Porosity | $\phi$ | 0.10 | 0.20 | – |
| Permeability in x-direction | $k_x$ | 10 | 1000 | mD |
| Permeability in y-direction | $k_y$ | 10 | 1000 | mD |
| Permeability in z-direction | $k_z$ | 10 | 10 | mD |
| Bulk heat capacity | $c_b$ | 2300 | 2450 | $\frac{\text{kJ}}{\text{m}^3*\text{K}}$ |
| Bulk heat conductivity | $\lambda_b$ | 0.190 | 0.260 | $\frac{\text{kJ}}{\text{m}*\text{day}*\text{K}}$ |

bulk heat capacity, and conductivity. The $p_1$ and $p_2$ values of the modelled properties are presented in Table 1.

$$p = a + be^{\left(-\frac{(x-c)^2}{d^2}\right)} \tag{2}$$

where $a = p_1$, b are the fractional addition to the minimum property value in the $x$-direction, c is the location in the $x$-direction, where the maximum value of the modelled property occurred (i.e., the Gaussian peak) and $d = p_2 - p_1$ represents the width of the Gaussian trend. Here we opted for $a = p_1$, $b = p_2 - p_1$, $c = 125$, $d = 40$.

The geological models establish spatial heterogeneity in a selected property with a trend. The heterogeneity translated to different absolute values of reservoir properties. Table 1 presents all the properties used for geothermal reservoir modelling. The visual representation of porosity, permeability in $x - y$ directions, bulk heat capacity, and bulk heat conductivity of the two geothermal models are shown in Figs. 2,3.

### 2.3. Well density function

#### 2.3.1. From regular to flexible well patterns

In this study, we propose using well patterns typical for oil and gas field development for geothermal field development. We experimented with a line-drive well pattern, a large-scale extension of doublet wells [7,30]. We also tested 5-spot patterns, consisting of an injection well in the centre and four surrounding producer wells. Onwunalu et al. [9,24] have extensively studied well pattern operators that distort the shape, size, orientation, type, and well locations. Here, we aim to use regular well patterns as introduced by Onwunalu et al. [9], like line-drive and 5-spot and distort their shape by resizing them. The arguments of the resizing operator were the horizontal/lateral $(PS_x, y)$ distance between two injectors. A regular pattern denoted a globally constant $(PS_x = PS_y)$ injector-to-injector distance in the reservoir domain.

For the development of heterogeneous reservoirs, we suggest proof of concept of a flexible well placement strategy. The heterogeneity refers to the porosity, permeability, heat capacity, and conductivity of the reservoir in different directions. We opted to model a property with a function as discussed in the Geothermal Geological Models. We considered a well-density function that directly responds to the 1-dimensional geological trends.

#### 2.3.2. Well density function

We propose two flexible well pattern scenarios, described with Eqs. (3),(4) for the linear and the Gaussian trend, respectively.

$$WDF_{linear} = ax + b \tag{3}$$

$$WDF_{Gaussian} = c + cde^{\left(-\frac{(x-m)^2}{f^2}\right)} \tag{4}$$

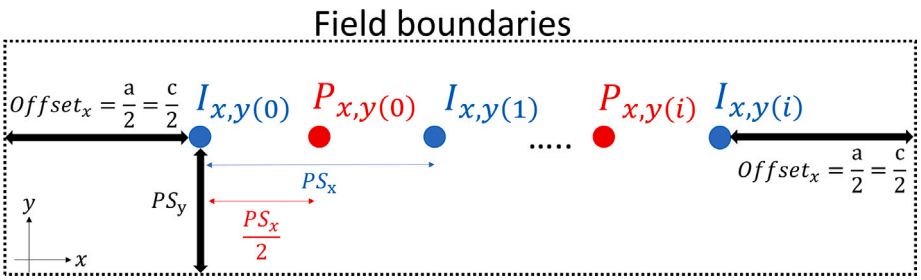


**Fig. 4.** Boundary conditions of well placement based on well density functions presented in Eqs. (3), (4). We note injectors in blue and producers in red. Parameters a, and c that define the offset or distance from the left or right field boundary are explained in Eqs. (3), (4) respectively.

In Eq. (3), a is the fractional reduction of pattern size from its initial size $b$, measured in grid blocks. In Eq. (4), $c$ is the normal or maximum pattern size in the $x$-direction, $c * d$ is the fractional increase or reduction of pattern size in the $x$-direction from the normal pattern size $c$, m is the location in the $x$-direction where the channel peak is encountered, and $f$ represents the width of the Gaussian curve. $c, d, m, f$ are measured in grid blocks, and $c * d$ takes values between 0 and 1.

Well placement (Fig. 4) was initialised with an injection well at an offset from the origin of the $x$-axis, which is $a/2$ and $c/2$ for the linear and Gaussian well patterns, respectively. The offset for both well patterns ensures a commensurate field area for optimisation for both geological models. The x-location value of the second injector ($x_{inje(i+1)}$) occurred from the addition of the absolute value of the x-location of the first injector to the x-location of the first injector. The process continued until an injector location fell out of the field boundaries minus a minimal distance of $a/2$ and $c/2$ for linear and Gaussian well-density functions, respectively. Production wells were placed in the middle of the distance of two injectors based on Eq. (5).

$$x_{prod(i)} = \frac{x_{inje(i)} + x_{inje(i+1)}}{2} \tag{5}$$

We ensured that one producer was always placed between two injectors. If the last producer was placed outside the field boundaries, we did not consider it in the development strategy (Eq. (6)). We utilised the resizing well-shape operator to assign the y-location of injectors and producers with equidistant spacing.

$$x_{prod(i)} - x_{inje(i)} = \left(x_{inje(i+1)} - x_{inje(i)}\right) * \frac{x_{inje(i)}}{x_{inje(i)} + x_{inje(i+1)}} \tag{6}$$

### 2.4. Objective function and optimisation

#### 2.4.1. Delft Advanced Research Terra Simulator (DARTS)

We carried out the simulations with the Delft Advanced Research Terra Simulator (DARTS), developed at Delft University of Technology [31,32]. Furthermore, linearisation in DARTS was implemented using the Operator-Based Linearisation approach (OBL) [33–36]. The successful application of OBL in flow simulations has been demonstrated by several researchers [33–37]. Geothermal reservoir simulations included conservation of mass, conservation of energy, and Darcy's Law for fluid flow in porous media [38].

#### 2.4.2. Reservoir simulation

The geothermal reservoir simulations require the geology of the simulated field and the well density function as input. Additionally, we present the set-up of the simulations in Table 2. We imposed a fixed volumetric rate control on the wells and not bottom hole pressure (BHP) constraints, to balance the injected and produced volume of geothermal fluid, which is a regulation in geothermal operations to maintain mass balance in the reservoir after extracting the heat from the fluid. We used different injection rates adapted to the two geological models, as well, due to the convergence restrictions of the simulator. Furthermore, large-volume boundary cells are used at the edge of the domain to imitate an open-to-flow reservoir.

**Table 2**
Constant parameters used as simulation inputs, in reservoir models.

| Constant | Annotation | Value | Unit (SI) |
|---|---|---|---|
| Reservoir x,y-discretisation | nx, ny | 250 | Grid blocks |
| Reservoir z-discretisation | nz | 1 | Grid blocks |
| Grid x,y-dimension | dx, dy | 40 | m |
| Grid z-dimension | dz | 50 | m |
| Reservoir top depth | $d_{top}$ | 2200 | m |
| Reservoir bottom depth | $d_{bottom}$ | 2250 | m |
| Initial reservoir temperature | $T_{res}$ | 349.15 | K |
| Initial reservoir pressure | $P_{res}$ | 24.2 | MPa |
| Injection temperature | $T_{inj}$ | 308.15 | K |
| Injection rate$_{linear}$ | $Q_{inj}$ | 3000 | $\frac{m^3}{day}$ |
| Injection rate$_{Gaussian}$ | $Q_{inj}$ | 2000 | $\frac{m^3}{day}$ |
| Injection/Production well depth | $d_{inj/prod}$ | 2225 | m |
| Project lifetime | t | 30 | years |
| Fluid density | $\rho_f$ | 1000 | $\frac{Kg}{m^3}$ |
| Fluid heat capacity | $c_f$ | 4200 | $\frac{kJ}{m^3 * K}$ |
| Fluid heat conductivity | $\lambda_f$ | 0.730 | $\frac{kJ}{m*day*K}$ |
| Boundary cell volume inflation factor | v | $10^6$ | – |

We calculate the energy produced/injected per well ($E_{pro/inj}$) and net energy recovered ($E_r$) with Eqs. (7),(8) where t stands for the evaluation interval of the simulation, $\Delta t$ is the project lifetime and $N$ is the number of wells. Note that we do not consider any pressure-related energy consumption, unlike Zaal et al. [28].

$$E_{pro/inj} = \frac{E_{pro/inj}(t+1) - E_{pro/inj}(t)}{\Delta t} \tag{7}$$

$$E_r = \sum_{t=0}^{\Delta t}\left(\sum_{n=0}^{N} E_{pro} * t - \sum_{n=0}^{N} E_{inj} * t\right) \tag{8}$$

#### 2.4.3. Economic model

The economic modelling of geothermal developments under Dutch fiscal conditions has been extensively studied in the past [1,28,39,40]. Drilling costs generally account for a significant part of expenditure on geothermal projects. In this study, we included only these expenses to simplify the calculations, operational costs (OpEx) are not included. Drilling costs vary for each well depending on the depth, given in Eq. (9) [41], in which d is the measured depth in meters ($m$) and the well costs are in Euros (€). The output of the equation is the well and installation costs of a single well multiplied by the total number of wells and accounts for the total Capital Expenditures (CapEx).

$$CapEx = C_w = N_w * (375000 + 1150d + 0.3d^2) \tag{9}$$

Revenues generated from heat recovered ($E_r$) contribute to the income of geothermal projects. The economic model is built based on the heat price P derived from [42] for the year 2020 ( Table 3). We

**Table 3**
Constant parameters used as simulation inputs, in reservoir models.

| Constant | Annotation | Value | Unit (SI) |
|---|---|---|---|
| Heat price$_{base}$ | p | 51.8 | €/MWh |
| Heat price$_{low}$ | p | 30 | €/MWh |
| Project lifetime | $\Delta t$ | 30 | Years |

calculate the undiscounted cash flow ($CF_t$) from Eq. (10) derived from Zaal et al. [28]. We note cashflow as $CF_t$ (€), $\Delta t$ is the project lifetime in years:

$$CF_t = \sum_{t=0}^{\Delta t} CF \tag{10}$$

Zhang et al. [27] established the cashflow calculation with Eq. (11), where $E_r$ are the heat revenues and CapEx are the capital expenditures:

$$CF = E_r - CapEx \tag{11}$$

#### 2.4.4. Optimisation

We utilised the Simplicial Homology Global Optimisation (SHGO) algorithm [43–45] to optimise cashflow using the pattern size or the well density function as an input for the objective function. SHGO is appropriate for solving global and derivative-free, black-box optimisation problems. The algorithm is specialised in finding all the local minima of non-smooth objective functions with expensive function evaluations efficiently, which is especially suitable in our research given the non-smooth nature of the objective function presented in Fig. 5. Please refer to Table 4 for all the parameters used in the optimisation process for both geological models and well density function. The stopping criteria of the optimisation were the maximum number of iterations stated in Table 4. The convergence criteria utilised the default setup of the optimiser, which balanced computational efficiency and accuracy.

#### 2.4.5. Thermal recovery

The energy present in the reservoir fluid of the geothermal models refers to a temperate difference between the initial reservoir (fluid and rock) temperature and injection fluid temperature [46]. In this case, it is $\Delta$T=51 °C, and we accounted only for the energy stored in the reservoir fluid. We did not consider the thermal recharge of the reservoir by the over and underburden. The energy stored in the fluid is calculated based on Eq. (12)

$$E_f = \Delta T * C_f * V_f \tag{12}$$

where $E_f$ is the energy of the fluid stored in the reservoir measured in GJ, $C_f$ is the volumetric heat capacity of the fluid measured in $\frac{kJ}{m^3 * K}$ and $V_f$ is the volume of the fluid noted in $m^3$.

## 3. Results and discussion

### 3.1. Geological model with Gaussian trend

#### 3.1.1. Analytical search of optimal regular well pattern

We performed a manual search of all well pattern sizes with integer pattern size values to find the optimum regular well patterns with two development scenarios: a regular line-drive and a regular 5-spot well pattern. The manual process included a grid block-by-grid block evaluation of the objective function and not assigning decimal numbers, leading to a step-wise gap of 40 m that was not evaluated.

The minimum pattern size applied to this geological model was 5 grid blocks, which correspond to 200 m. Fig. 5 illustrates the response curves of the search for the development scenarios. The optimal development strategy of regular well patterns is the 5-spot well pattern, which delivers the most profitable development. The optimised pattern size is 320 m ($nx = ny = 8$ grid blocks). Furthermore, we observe the non-smooth nature of the objective function, which stems from the number of injectors and producers. Specifically, the smaller the pattern size, the more rows of injectors and producers fitted in the simulated reservoir. The small pattern sizes impact the CapEx negatively and the energy produced positively, leading to an irregular behaviour of the response function.

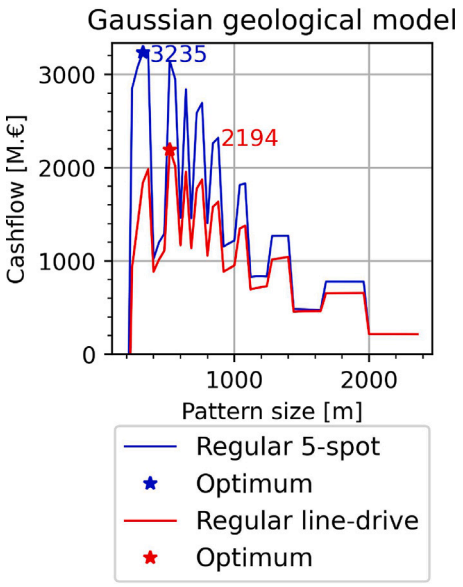


**Fig. 5.** Response curves development strategy with regular well patterns. The optimal pattern size per development scenario is noted in the plot with a star per well pattern. We note the non-smooth nature of the objective function.

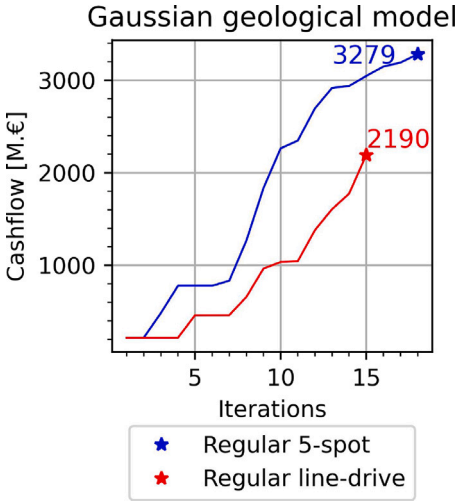


**Fig. 6.** Optimisation results per development strategy with a regular well pattern. The optimal pattern size per development scenario is noted in the plot with a star.

#### 3.1.2. Numerical optimisation with regular well patterns

We numerically optimised the same geological model with a regular line-drive and 5-spot well pattern. The optimised development strategies suggest that a regular 5-spot well pattern delivered the highest NPV. Fig. 6 delineates the optimisation result per development scenario. The optimal pattern size is 340 m injector to injector distance or $nx = ny = 8.5$ grid blocks.

After 30 years of production, almost all the reservoir cools down close to the injection temperature. A rim of unswept hot water is present on the north and east sides due to boundary conditions applied in well placement that do not allow more wells to be placed in those areas. Additionally, we have imposed inflation of the fluid volume present

**Table 4**
Numerical and field values of optimisation parameters.

| Annotation | Numerical value | Unit | Field value | Unit |
|---|---|---|---|---|
| a | [3, 120] | Grid blocks | [120, 4800] | m |
| b | [3, 120] | Grid blocks | [120, 4800] | m |
| c | [5, 55] | Grid blocks | [200, 2200] | m |
| c*d | [0, 1] | – | [0, 1] | – |
| m | [80, 170] | Grid blocks | [320, 6800] | m |
| f | [10, 70] | Grid blocks | [400, 2800] | m |
| $PS_y$ - linear | [3, 60] | Grid blocks | [120, 2400] | m |
| $PS_y$ - Gaussian | [5, 55] | Grid blocks | [200, 2200] | m |
| iterations - linear | 300 | | | |
| sampling points - linear | 50 | | | |
| iterations - Gaussian | 900 | | | |
| sampling points - Gaussian | 200 | | | |

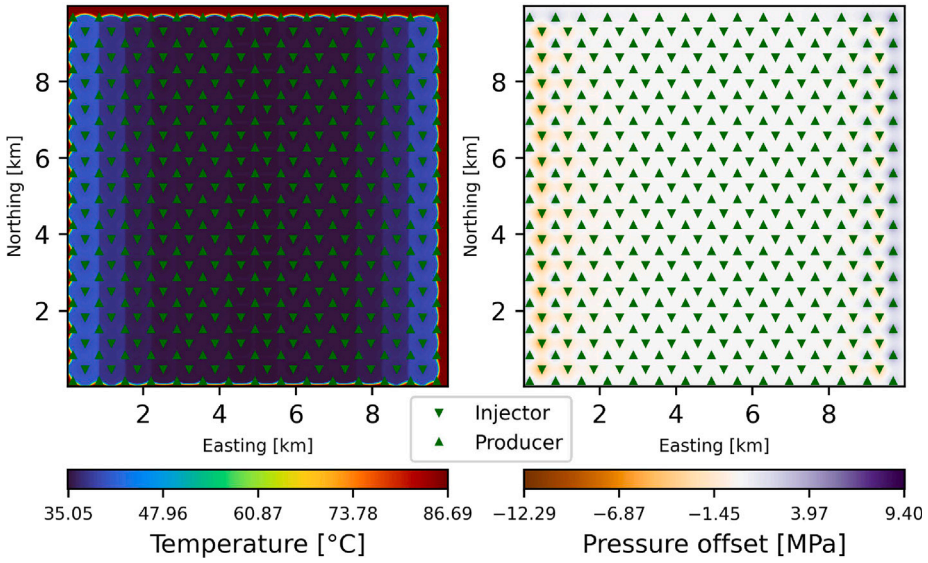


**Fig. 7.** Numerically optimised development strategy with a regular 5-spot well pattern for the geological model with the Gaussian trend. Left: Field temperature distribution after 30 years of production. Right: Pressure offset of BHP from initial reservoir top pressure = 24.2 MPa after 30 years of production.

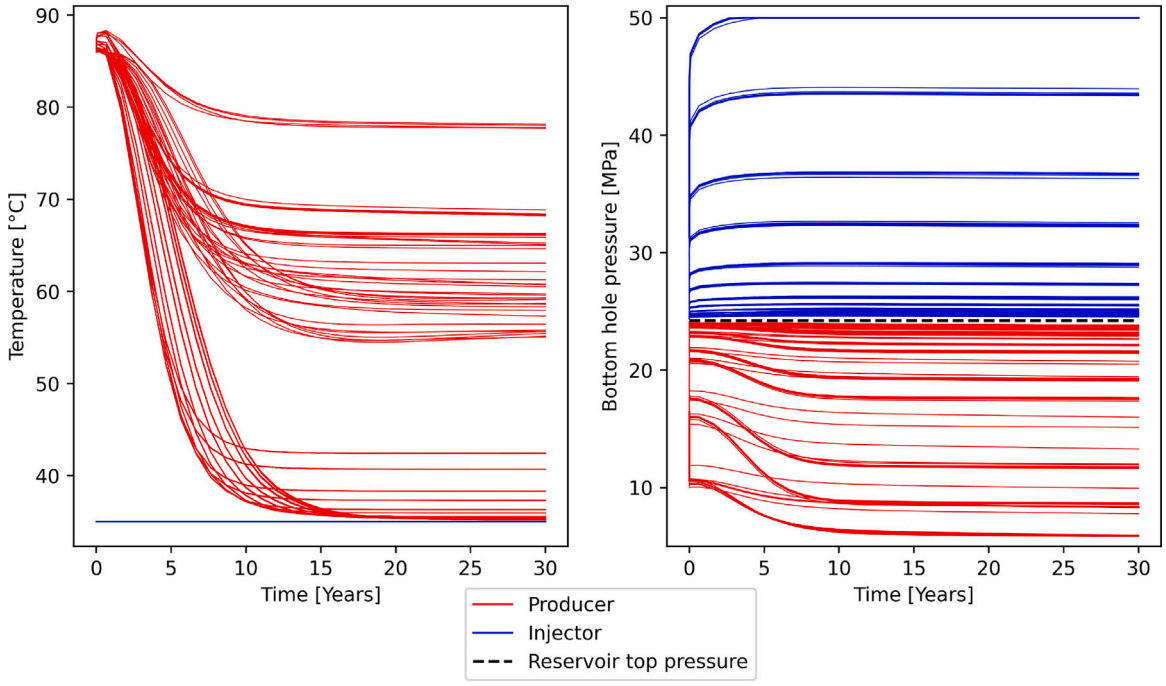


**Fig. 8.** Numerically optimised development strategy with a regular 5-spot well pattern for the geological model with the Gaussian trend: Temperature and bottom hole pressure time series per well. Red curves correspond to production wells and blue to injection.

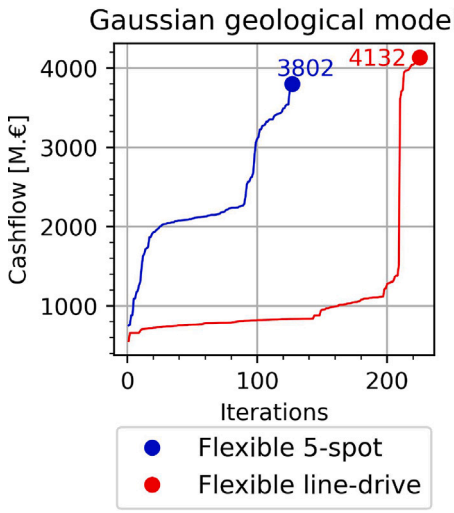


**Fig. 9.** Optimisation results for the development strategies with a flexible well pattern. The optimal pattern size per development scenario and geological model are noted in the plot.

at the boundaries of the reservoir hence the production wells present there will exhibit non-realistic time-series of production temperature profile. Fig. 8 shows that a group of production wells encounter a cold front of 35-45 °C after ten years of production. In contrast, the rest stabilise at a temperature range of 60-80° C after 15 years of production, given that they are placed close to the boundaries where the volume of the hot reservoir fluid is inflated, therefore the cooling effects are masked. All well temperature profiles stabilise after 15 years of production.

Pressure field data confirm that the areas with low porosity-permeability experience the most significant pressure offset from the initial reservoir top pressure (Fig. 7). The bottom hole pressure time series suggests a significant pressure offset for both injectors and producers. The pressure offset for the injection wells stabilises at similar times, however at different pressure values. Production wells exhibit values lower than the initial reservoir pressure and appear to stabilise each at different times. After 10 years of production bottom hole pressure reaches a plateau for all wells. We also observe the clustering of production wells based on temperature both after 15 years of production.

#### 3.1.3. Numerical optimisation with flexible well patterns

We numerically optimised the objective function for this geological model with a flexible line-drive and 5-spot well pattern. The optimised development strategies suggested that the line-drive well pattern returns the highest cashflow in contrast to the previous setup, where the 5-spot exhibited better performance. For the Gaussian model, the well-density function describing the optimal pattern size (in km) distribution in the $x$-direction is described with Eq. (13). The optimal pattern size for the $y$-direction is 128 m ($ny = 3.2$ grid blocks). See Table 2 for $nx$ and $dx$ values. Fig. 9 shows the optimisation results for the flexible well patterns. The development scenario with line-drive well patterns outperforms the 5-spot when numerically optimised.

$$f_{wd,gauss(x)} = 2.032 * (1 + 0.1225) * e^{\left(-\frac{(x-5.428)^2}{0.953^2}\right)} \quad (13)$$

Fig. 10 shows the thermally unswept areas at the west and east sides of the reservoir after 30 years of production as a result of well placement boundary conditions. Fig. 11 presents that temperature breakthrough starts between 5–10 years of production. We observe a clustering of wells where breakthroughs start after five years of production, associated with high permeability areas, but the temperature did not drop below 60 °C after 30 years of production, due to the boundary conditions. The wells that experience the breakthrough between 10–15 years encounter temperatures up to 35 °C after 30 years of production and represent the areas with lower permeability.

Reservoir top pressure offsets negatively around injection well and positively on production wells. Note that the areas where the boundary producers lay have low porosity and permeability hence pressure elevates. We observe minimal pressure offset around the producers that lie in the middle of the reservoir where there is substantial permeability. We observe a drop in the bottom hole pressure profile in all wells that instantly initiates upon production and stabilises after 15 years of production. After that, BHP stabilises, though there is a clustering of the final BHP value due to the well location and boundary reservoir conditions. We also observe a variable behaviour of clustered production wells with varying temperature breakthroughs of 0, 5, and 15 years.

### 3.2. Geological model with linear trend

#### 3.2.1. Analytical search of optimal regular well pattern

Similar to the description in the methodology for the geological model with the Gaussian trend, we performed a manual search to find the optimum regular well patterns with two development scenarios: a regular line-drive and a regular 5-spot well pattern. The optimum pattern size found is 3 grid blocks, translating to 120 m of injector-to-injector distance in both x- and $y$-direction for this geological model. Fig. 12 illustrates the response curves of the exhaustive search. The optimal development strategy was the 5-spot well pattern, which is the most profitable, with the optimised pattern size being 240 m ($nx = ny =$ 6 grid blocks) injector to injector (x,y directions) distance.

#### 3.2.2. Numerical optimisation with regular well patterns

We numerically optimised the same geological model with a regular line-drive and 5-spot well pattern. The optimised development strategies suggest that a regular 5-spot well pattern delivered the highest cashflow. Fig. 13 delivers the optimisation result per development scenario. The optimal pattern size for the linear model is 236 m injector to injector distance ($nx = ny = 5.9$ grid blocks) for the linear model.

After 30 years of production, only the north and east boundaries of the reservoir remain thermally unswept due to the boundary conditions applied in well placement. Fig. 15 shows that thermal breakthrough occurs instantaneously after the beginning of the production a temperature stabilises between 5–10 years. However, one group of wells encounters a 35–40 °C thermal front and the second a temperature range of 60–80 °C front.

Pressure field data suggest that the eastern part of the reservoir, with its low porosity-permeability, experiences the greatest pressure increase from the initial reservoir pressure (Fig. 14). However, given that part of the reservoir is subject to fluid volume inflation we do not consider this as a realistic reservoir response to fluid injection. The bottom hole pressure profile exhibits a variable response as well with a great range of pressures. Interestingly all pressure values stabilise after 5 years of production. Finally, we observe clustered production wells where temperature breakthroughs occur right after production and settle after 5 years at different temperatures.

#### 3.2.3. Numerical optimisation with flexible well patterns

We numerically optimised both geological models with a flexible line-drive and 5-spot well pattern. The optimised development strategies suggest that the line-drive well pattern returns the highest cashflow (Fig. 16). The well-density function describing the optimal pattern size (km) distribution in the $x$-direction is described with Eq. (14) for the linear model. The optimal pattern size for the $y$-direction is 128 m ($ny = 3.2$ grid blocks). See Table 2 for $nx$ and $dx$ values.

$$f_{wd,lin} = \frac{4.409}{nx * dx} * x + 0.977 \quad (14)$$

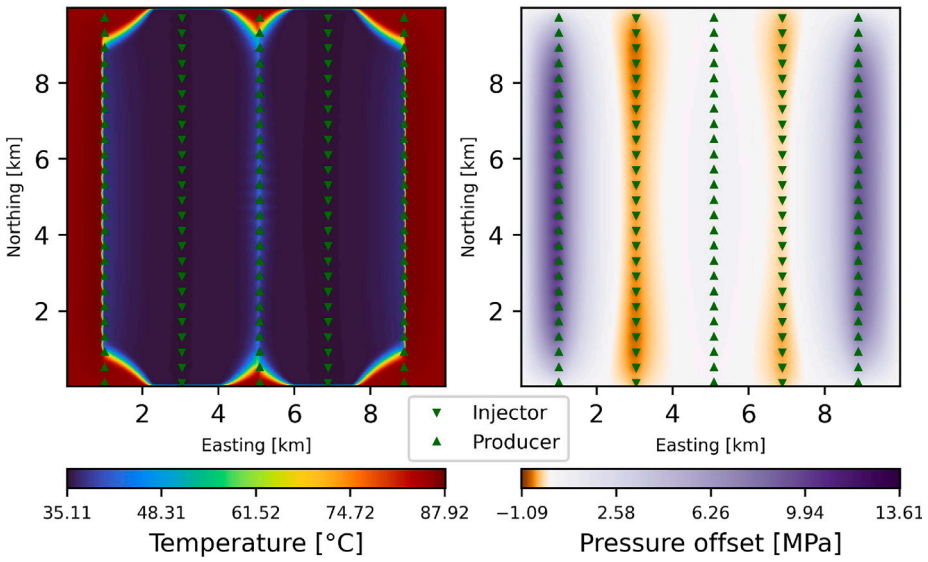


**Fig. 10.** Optimised development strategy with a flexible line-drive well pattern for the geological model with the Gaussian trend. Left: Field temperature distribution after 30 years of production. Right: Pressure offset of BHP from initial reservoir top pressure = 24.2 MPa after 30 years of production.

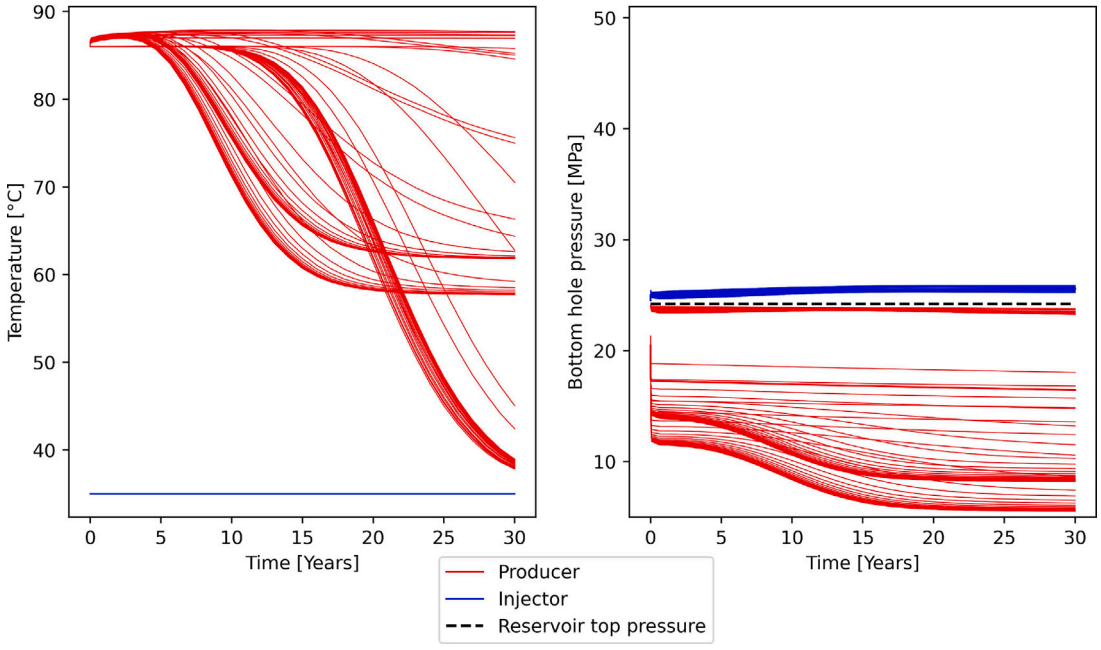


**Fig. 11.** Optimised development strategy with a flexible line-drive well pattern for the geological model with the Gaussian trend: Temperature and bottom hole pressure time series per well. Red curves correspond to production wells and blue to injection.

After 30 years of production, the most porous and permeable part of the reservoir is cooled down by the injected water. We observe thermally unswept areas at the west and east sides of the reservoir due to the well placement restrictions at the reservoir boundaries (Fig. 17). Temperature breakthrough occurs irregularly between different wells, depending on their location (Fig. 18). There is a distinct clustering of wells based on the thermal time-series profile as well. The thermal front profile does not settle until 15 years of production. After that, we observe temperature variability from the reservoir temperature to the actual injection temperature. Several wells do not drop below 60 °C after 30 years of production.

Field pressure data suggest that the eastern and least porous-permeable parts of the reservoir exhibit the highest pressure offset from the initial reservoir pressure. The mass of the fluid that circulates in those low permeability areas to be produced potentially perturbed the pressure field. The bottom hole pressure time series (Fig. 18) suggests that production pressure deviates after 5 years of production for all wells and settles after 15 years of production. There is variability

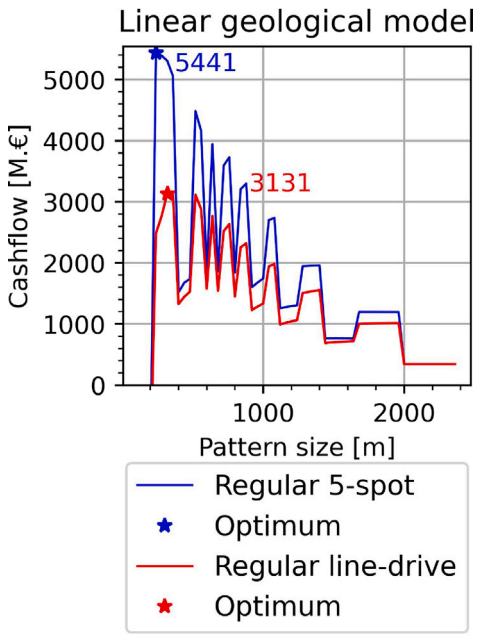


**Fig. 12.** The response curve of the analytical, objective function solution for both development strategies with a regular well pattern. The optimal pattern size per development scenario is noted in the plot.

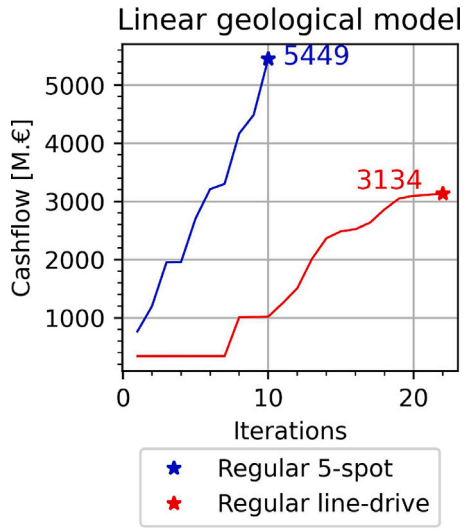


**Fig. 13.** Optimisation results of both geological models and development strategies with a regular well pattern. The optimal pattern size per development scenario and geological model are noted in the plot.

between the BHP values for all wells depending on their location and reservoir porosity and permeability values.We additionally observe a variable behaviour of clustered production wells with varying temperature breakthroughs of 0, 5, and 15 years. Each cluster stabilises at different temperatures.

#### 3.2.4. Implications of lower heat price on optimised, flexible well patterns

We set up the optimised development strategies with a heat price valid for 2020 [42]. A reassessment of the optimisation performance of flexible line-drive well patterns with a heat price of 30 €/MWh demonstrates that a 42% reduction in heat price introduces a 46% drop-down in the cashflow of the development (Fig. 19). Therefore, a lower heat price than the already applied reduces the economic performance but still yields a profitable development of flexible well patterns than the regular line-drive well pattern. Subsequently, geothermal developments with flexible well patterns are favourable under lower heat price than the invesigated one. We suggest further investigation to identify the minimum required heat price that would yield the developments profietable as well as accounting for heat price uncertainty.

**Table 5**
Discrepancies in stored energy in the fluid [in PJ] for both geological models, between the cases of the boundary cells are inflated in volume by a factor of $10^6$ or not.

| | Linear trend | Gaussian trend |
|---|---|---|
| Fluid energy [PJ] | 160 | 145 |

### 3.3. Energy recovered

The total energy stored in the pore fluid of each reservoir model is illustrated in Fig. 20. Note that we inflated the volume of the grid cells at the rim of the reservoir by a factor of $10^6$, introducing volume inflation of the fluid present in those cells ( Table 5). Fig. 20 does not include the inflated numerical cells so we can clearly visualise the 2D lateral variation of the energy stored in the reservoir. The energy stored in the fluid of the geological model with a linear trend is 160 PJ, and in the geological model with a Gaussian trend, it is 145 PJ, when we do not include those boundary cells. Most of the energy is stored in the high porosity areas for both reservoir models. The recovered energy of the optimised development strategies per geological model is presented in Table 5. The application of an optimised, flexible line-drive pattern increases the energy recovered for the geological model with the linear trend. In contrast, the application of flexible well patterns in the geological model with a Gaussian trend does not guarantee the optimal energy recovered even though it improves cashflow (Fig. 21).

### 3.4. Comparison of optimised regular and flexible well patterns

The results present a consecutive improvement in cashflow from the manual search to numerically optimised regular well patterns and to numerically optimised flexible well patterns. The manual search for the response of the objective function delivers the least profitable development scenarios with regular 5-spot well patterns for both geological models. The numerical optimisation method with regular well patterns improves the cashflow compared to the manually found optimum solution but suggested the 5-spot as the optimal decision for both geological realisations. The difference in cashflow between the numerical and analytical methods is minimal (Fig. 22). The numerical method could capture a better optimum than the analytical search as it assigned decimals in the parameter search space instead of only integers.

The numerically optimised flexible well pattern methodology successfully adapts the pattern size based on the underlying heterogeneity of the subsurface. The optimised pattern sizes in areas with the highest porosity values in the developed field exhibit higher values compared to regions with low porosity. Additionally, the optimised, flexible well patterns not only significantly increase the cashflow but also introduce that the line-drive pattern is the optimal development in contrast to what optimised regular well patterns suggested. However, the difference was insignificant (Fig. 22).

### 3.5. Discussion of optimised development strategies

#### 3.5.1. Temperature and pressure

For the geological model with a Gaussian trend, pressure field data after 30 years of production indicate that the optimised, flexible line-drive well pattern induces a lower negative pressure offset concerning the area where injection wells were located, compared to the regular 5-spot. The area with production wells experiences approximately the same pressure decrease for both optimised regular 5-spot and flexible line-drive well patterns. We conclude that flexible well patterns induce

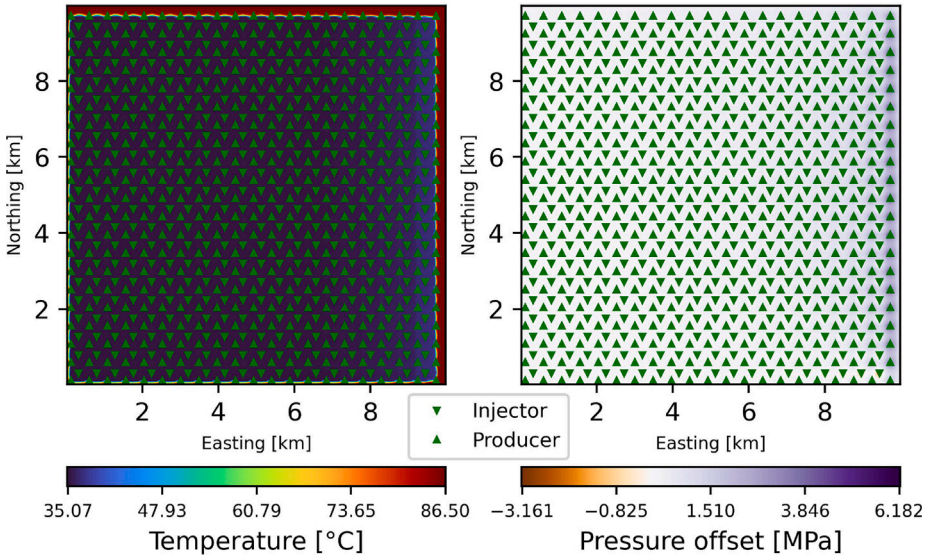


**Fig. 14.** Numerically optimised development strategy with a regular 5-spot well pattern for the geological model with the linear trend. Left: Field temperature distribution after 30 years of production. Right: Pressure offset from initial reservoir top pressure = 24.2 MPa after 30 years of production.

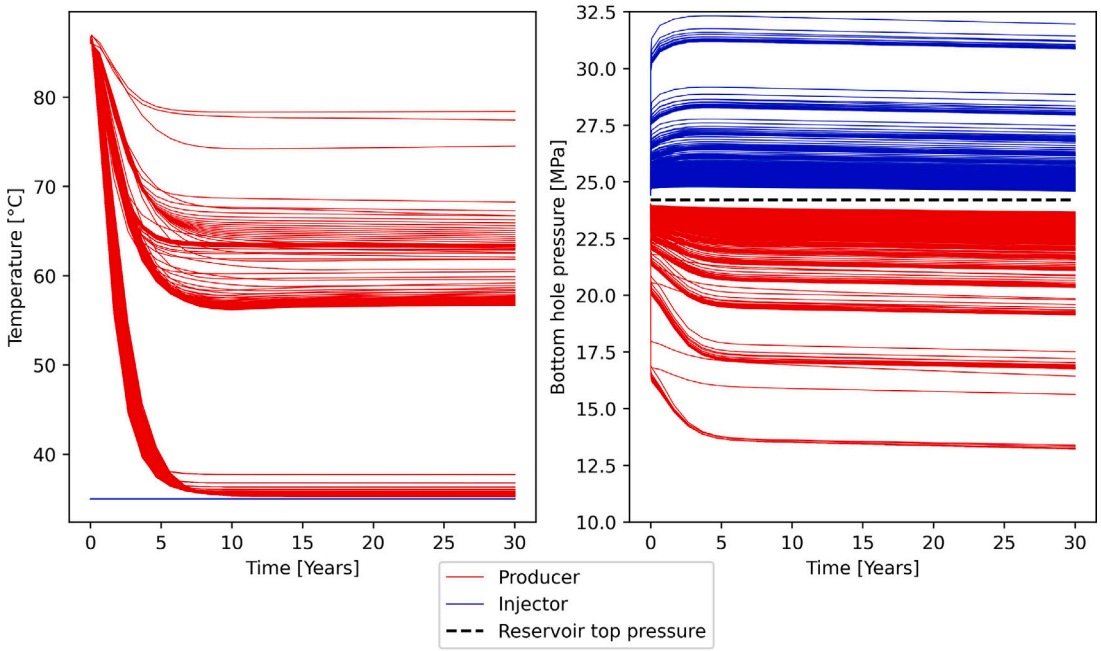


**Fig. 15.** Numerically optimised development strategy with a regular 5-spot well pattern for the geological model with the linear trend: Temperature and bottom hole pressure time series per well. Red curves correspond to production wells and blue to injection.

a narrower pressure deviation range than the regular 5-spot. We explain this observation with a lower number of wells in the field developed with a flexible well pattern compared to the regular well pattern. Temperature-wise, the optimised 5-spot partially thermally sweeps the reservoir after the first ten years of production. The optimised flexible line-drive pattern imposes a temporal delay on the arrival of the cold front on the production wells, which favour a longer-term energy utilisation.

Field pressure data for the geological model with a linear trend, optimised with a flexible line-drive well pattern, indicate that the injection wells not surrounded by producers increase the pressure field around them, compared to the optimised regular 5-spot. Consequently, when injectors are placed alone regionally, they increase the reservoir pressure since they locally introduce more fluid in the subsurface. The pressure drop around production wells does not vary significantly for both geological models. Flexible well patterns impose smaller extrema on bottom hole pressure than the regular well patterns. The temperature time series of flexible line-drive show a cold front breakthrough postponed by at least ten years compared to the regular 5-spot and simultaneously increased cashflow.

The application of the flexible well patterns for both geological realisations suggests smaller extrema in the pressure offset from the initial reservoir pressure in combination with a temporal delay of the thermal breakthrough, compared to the regular well patterns. Moreover, flexible well patterns are a promising approach for operations with geomechanical constraints since they prove the ability to limit pressure variations after 30 years of production. It is worth mentioning that the presence of a pressure offset from the initial reservoir pressure accentuates the necessity of investigating potential geomechanical constraints in the context of induced seismicity in geothermal operations.

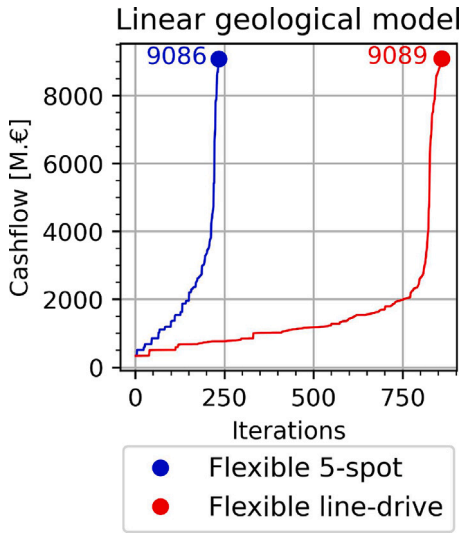


**Fig. 16.** Optimisation results for development strategies with a flexible well pattern. The optimal pattern size per development scenario is noted in the plot.

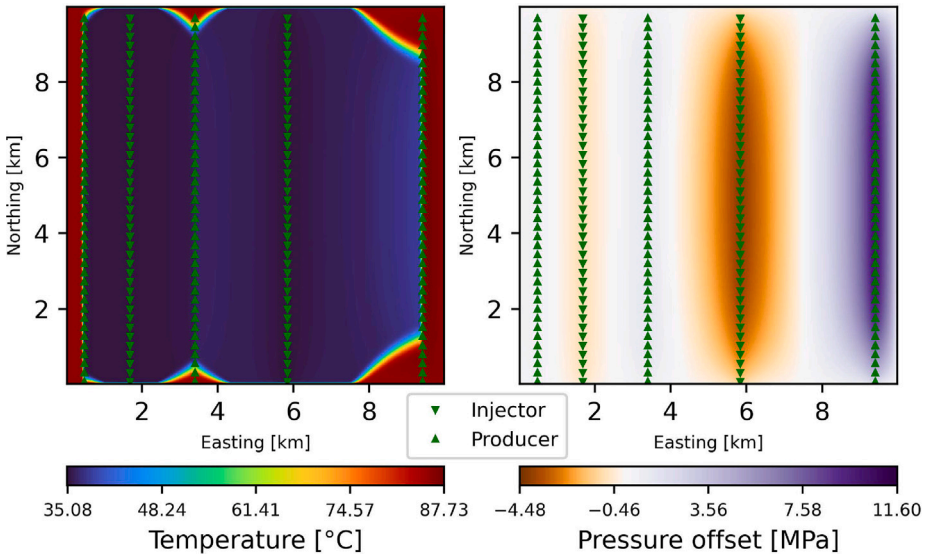


**Fig. 17.** Optimised development strategy with a flexible line-drive well pattern for the geological model with the linear trend. Left: Field temperature distribution after 30 years of production. Right: Pressure offset from initial reservoir top pressure = 24.2 MPa after 30 years of production.

Subsequently, including BHP constraints in the optimisation process (similar to [47]) in large-scale developments would further bring the research concept into a realistic perspective. Hence, we suggest numerically optimised flexible well patterns for large-scale geothermal exploitation if the operators target a long-term utilisation of the energy recovered combined with cashflow improvement, which aligns with the finding presented by Daniilidis et al. [47].

### 3.5.2. Energy recovered and cashflow

The energy recovered, evaluated in this study, refers to the energy recovered from the reservoir pore fluid for a given temperature difference between the reservoir and the injection fluid. For the geological model with a linear trend, the results support the initial hypothesis that the flexible well patterns directly increase the energy recovered from the geothermal development, which aligns with an increase in cashflow. The application of flexible well patterns on the geological model with the Gaussian trend inhibits the improvement of energy recovered. However, cashflow results suggest that the most profitable development does not necessarily produce the greatest amount of energy. This observation demonstrates that an objective function targeting optimised profitability is preferred over energy recovered in geothermal field development scenarios.

It is worth noting that the adopted geological models have different operational constraints. Specifically, the linear model uses a constant injection-production flow rate of 3000 $\frac{m^3}{day}$. The Gaussian model is operated with a flow rate of 2000 $\frac{m^3}{day}$. We imposed different flow rates per geological model because the forward simulations fail when high flow rates operate in a low transmissivity reservoir. Subsequently, we speculate that the lower flow rates directly relate to the sub-optimal behaviour of thermal recovery with flexible well patterns in the Gaussian geological model.

### 3.5.3. Beyond the proof of concept

We consider the current work as a proof of concept and we tested it on synthetic geological scenarios. We made specific choices regarding setting up realistic reservoir conditions, injection and production operational strategies, well patterns, well placement strategy, economic modelling and optimisation strategy to prove that flexible well patterns are more profitable than regular ones.

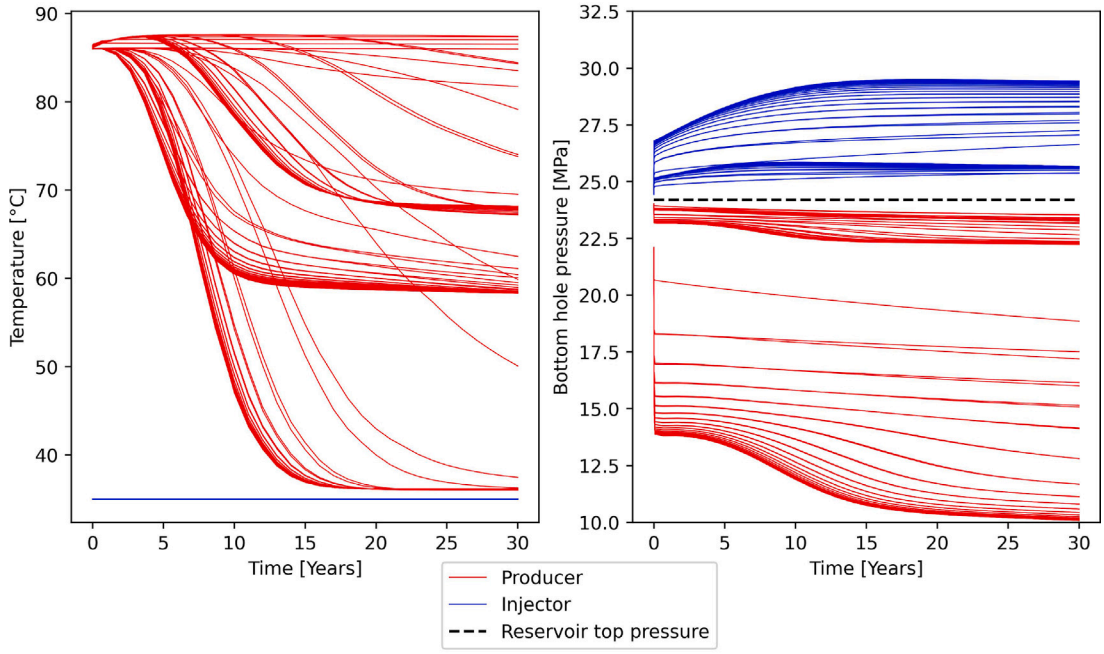


**Fig. 18.** Optimised development strategy with a flexible line-drive well pattern for the geological model with the linear trend: Temperature and bottom hole pressure time series per well. Red curves correspond to production wells and blue to injection.

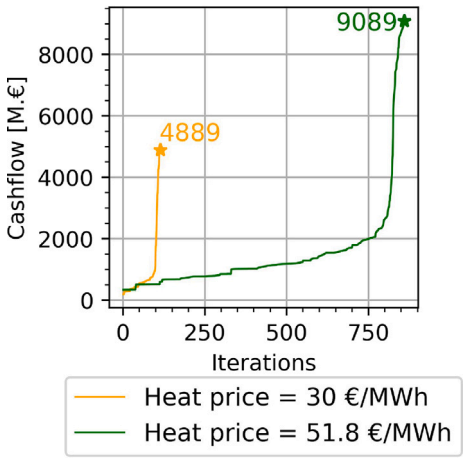


**Fig. 19.** Optimisation performance of flexible line-drive well pattern on geological model with linear trend under the adopted heat price of 30 €/MWh and the revised heat price of 51.8 €/MWh. A higher heat price increases cashflow but requires further iterations to reach the optimum hence is more computationally expensive than the lower heat price.

Concerning the geological test cases, we opted for two models that capture subsurface heterogeneities at least in 1 direction. The development of the synthetic geological scenarios was motivated by literature as described in the Methodology section. We recommend that this work be extrapolated to realistic geological models where property trends can be captured with a function. Furthermore, we set up realistic reservoir conditions similar to the ones encountered in the main geothermal matrix-flow-dominated reservoirs encountered in the Dutch subsurface [8]. We propose a follow-up on imposing different reservoir flow and thermal properties, (i.e. fracture-dominated flow), accounting for the thermal recharging of the reservoir from adjacent layers, incorporating faults in the reservoir, geomechanical constraints or geological uncertainty. When it comes to operational strategies we proposed and adopted specific injection and production strategies that are followed by Dutch geothermal operators [48]. We suggest a relevant adaption to the necessities of the local end-users, for example incorporating seasonal production of hot water depending on the demand of the market. Concerning the applied well patterns, there are numerous options for follow-up research similar to [24,49,50]. The application of well pattern operators (WPO) as discussed by Onwunalu et al. [49], could be a potential direction on a realistic test case as well. Here we selected the use of just two patterns and a single well pattern operator to capture and demonstrate the feasibility of the synthetic case study. The economic modelling is a crucial part of this study as well. We opted for a simplistic approach and incorporated only the well costs at the beginning of the geothermal field developments to generate cashflow on the geothermal development. Hence we kept a low-fidelity economic model for a proof of concept that could capture the necessary concepts without adding complexity to the results and their interpretations. For future work and realistic development scenarios, we recommend adding Operational Expenditures (OpEx) and Abandonment Expenditures (AbEx) to the model. That could be as a percentage of the CapEx or annually including different types of costs like maintenance of the facilities (wells, pipes, heat pump), permitting, water treatment etc. Additionally, the timing of the drilling of the wells could be step-wise and not instantaneous. Additionally, we would recommend discounting all expenditures and translating the investment to NPV. Also, we suggest that the optimisation target of cashflow translates to NPV. It would be beneficial to tune production and optimise it based on the seasonal demands and needs of the market. Finally, another potential direction that would promote research towards minimising the risk of induced seismicity in geothermal reservoirs, would be to create production and injection pressure constraints to avoid significantly perturbing the geomechanical balance of the subsurface.

## 4. Conclusions

This study first demonstrated that a spatial trend in a geological property was feasible to translate to a well density function that allowed the tuning of well placement. Additionally, it determined that optimal well placement is subject to the heterogeneity of the subsurface. Flexible well patterns are the result of this process. We optimised flexible well patterns that target the cashflow of geothermal developments, demonstrating improved profitability compared to regular oil and gas well patterns. The main findings from this research are:

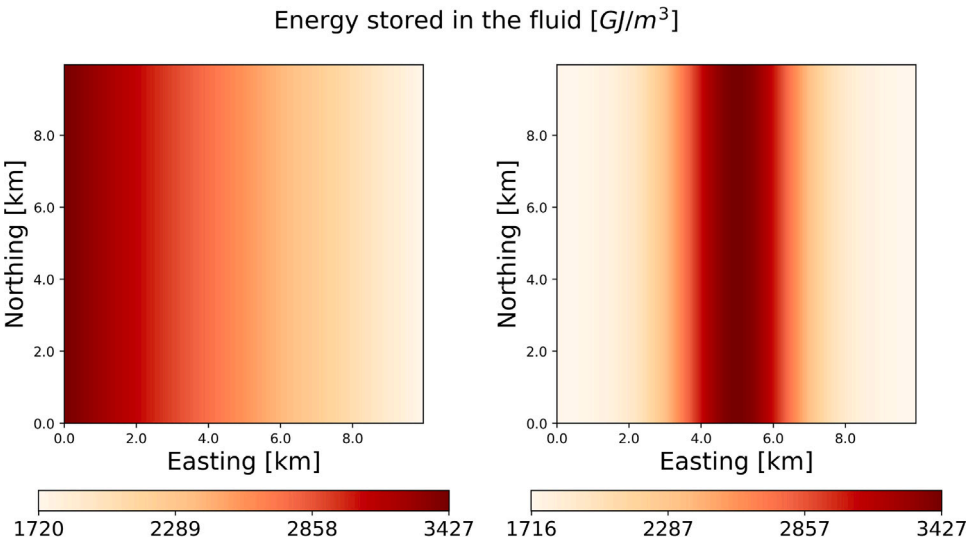


**Fig. 20.** Total amount of energy stored in the pore fluid for both reservoirs for a temperature difference of $\Delta$T=51°, assuming the reservoir is fully thermally swept and brought to injection temperature. The highest amount of energy stored is located in the areas with the highest porosity hence the volume of fluid present.

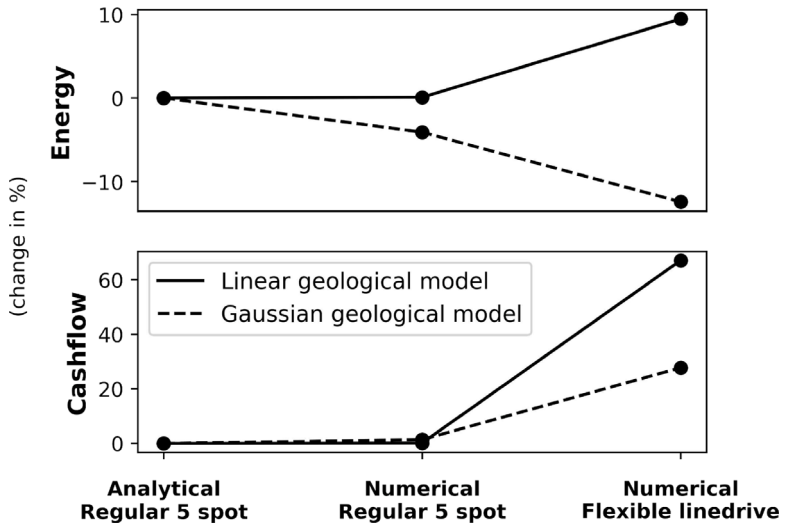


**Fig. 21.** Comparison of energy recovered and cashflow from the fluid recovered of optimised development strategies per optimisation methodology and geological model applied. When adopting flexible well patterns, the optimised cashflow does not necessarily coincide with optimal energy recovered.

- The application of optimised 5-spot and line-drive field development well patterns in large-scale synthetic geothermal field developments proved profitable for the tested geological models under the imposed operational and economic constraints.
- The optimal regular well development strategy for both geological models was the 5-spot pattern.
- Modelling well placement with a well density function, derived from a trend in a large-scale geological property, proved feasible and almost doubled the profitability by up to 70% and energy by 10%, depending on the geological scenarios.
- The application of flexible well patterns suggests that line-drive well placement is the most financially profitable large-scale geothermal field development strategy, unlike the adoption of regular well patterns.
- Cashflow improves with the application of flexible well patterns, in contrast to the energy recovered which is conditional to the geological setting.
- Flexible well patterns allow constrained pressure during production by up to 10 MPa and impose a temporal delay in the arrival of the cold front by approximately 10–20 years on the production

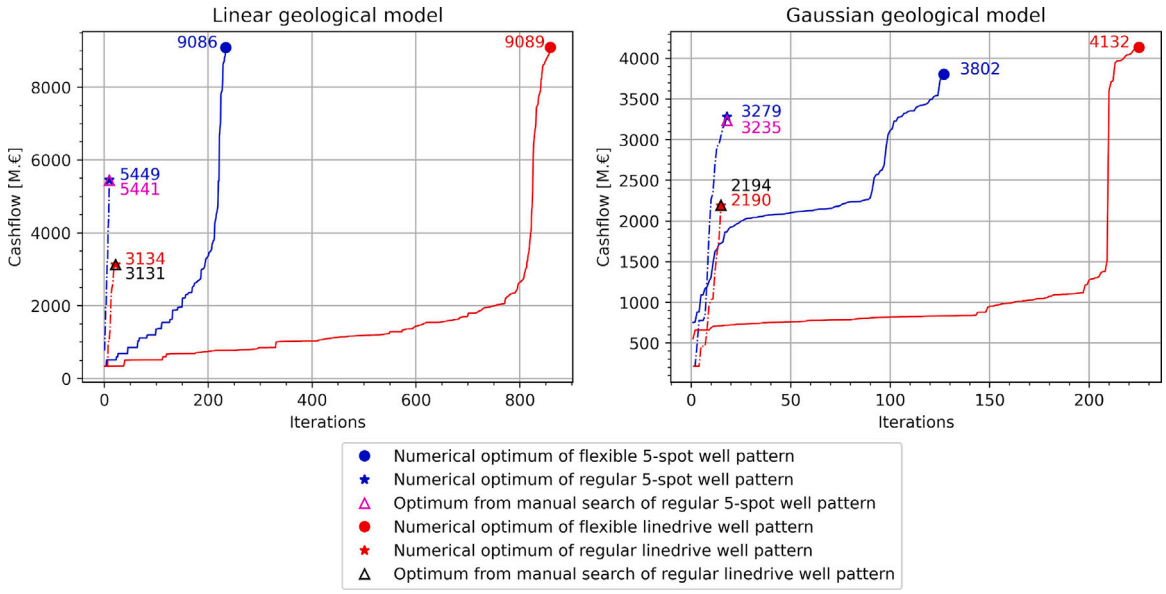


**Fig. 22.** Comparison of the different numerical and analytical methods used combined with flexible or regular well patterns that deliver the optimal cashflow for both geological models. Numerical methods require more iterations to converge to the optimum cashflow. Flexible linedrive well pattern are the most profitable for both geological scenarios.

wells depending on the geological setting. They favour a longer-term utilisation of the recovered heat assuming the undiscounted cashflow concept in this model.

Future recommendations for our research include the utilisation of realistic geology or even the introduction of uncertainty in geological realisations. Moreover, improving forward simulations by geomechanical and thermal constraints is necessary to comply with regulations for minimising the risk of induced seismicity. Multi-objective optimisation dealing with synchronously tuning flow rates, cashflow, sweep efficiency, pressure constraints, or even energy demand could benefit the application of the methodology and present the trade-off between these objectives.

## CRediT authorship contribution statement

**Entela Kane:** Writing – review & editing, Writing – original draft, Visualization, Validation, Software, Methodology, Investigation, Formal analysis, Data curation, Conceptualization. **Olwijn Leeuwenburgh:** Writing – review & editing, Validation, Supervision, Software, Methodology, Investigation, Conceptualization. **Gerard Joosten:** Writing – review & editing, Validation, Supervision, Methodology, Investigation, Conceptualization. **Alexandros Daniilidis:** Writing – review & editing, Supervision, Software, Methodology, Investigation. **David Bruhn:** Writing – review & editing, Supervision, Methodology, Investigation, Conceptualization.

## Declaration of Generative AI and AI-assisted technologies in the writing process

Statement: During the preparation of this work the author(s) used Grammarly Premium in order to improve the readability of the manuscript. After using this tool/service, the authors reviewed and edited the content as needed and took full responsibility for the content of the published article.

## Funding sources

This research did not receive any specific grant from funding agencies in the public, commercial, or not-for-profit sectors.

## Declaration of competing interest

The authors declare that they have no known competing financial interests or personal relationships that could have appeared to influence the work reported in this paper.

## Acknowledgements

Entela Kane would like to thank Dr. Anne Pluymakers for her mentorship while writing the manuscript. Moreover, the authors would like to thank the anonymous reviewers for their constructive feedback.

## Data availability

Data will be made available upon reasonable request.

## References

[1] F. Schoof, M. van der Hout, J. van Zanten, J. van Hoogstraten, Master Plan Geothermal Energy in the Netherlands, Stichting Platform Geothermie, Delft, The Netherlands, 2018.
[2] Ministry of Economic Affairs and Climate Policy, Pre-Publication Chapter 8, Natural Resources and Geothermal Energy in the Netherlands Annual Review 2020, Tech. Rep., 2021.
[3] H. Mijnlieff, A. Obdam, A. Kronimus, P.V. Hooff, Inhoudsopgave, Tech. Rep., 2009.
[4] C.J. Willems, H.M. Nick, G.J. Weltje, D.F. Bruhn, An evaluation of interferences in heat production from low enthalpy geothermal doublets systems, Energy 135 (2017) 500–512, http://dx.doi.org/10.1016/j.energy.2017.06.129.
[5] C.J. Willems, H. Nick, Towards optimization of geothermal heat recovery: An example from the West Netherlands Basin, Appl. Energy 247 (2019) 582–593, http://dx.doi.org/10.1016/j.apenergy.2019.04.083.
[6] S. Kahrobaei, R. Fonseca, C. Willems, F. Wilschut, J. Van Wees, Regional scale geothermal field development optimization under geological uncertainties, Eur. Geotherm. Congr. (2019).
[7] A. Daniilidis, H.M. Nick, D.F. Bruhn, Interference between geothermal doublets across a fault under subsurface uncertainty; implications for field development and regulation, Geothermics 91 (2021) 102041, http://dx.doi.org/10.1016/j.geothermics.2021.102041.
[8] C. Willems, Doublet Deployment Strategies for Geothermal Hot Sedimentary Aquifer Exploitation, TU Delft University (Ph.D. thesis), Delft University of Technology, 2017.
[9] J.E. Onwunalu, L.J. Durlofsky, A new well-pattern-optimization procedure for large-scale field development, SPE J. 16 (3) (2011) 594–607, http://dx.doi.org/10.2118/124364-PA.

[10] G. Liu, G. Wang, Z. Zhao, F. Ma, A new well pattern of cluster-layout for deep geothermal reservoirs: case study from the Dezhou geothermal field, China, Renew. Energy 155 (2020) 484–499, http://dx.doi.org/10.1016/j.renene.2020.03.156.
[11] D. Liu, J. Sun, The Control Theory and Application for Well Pattern Optimization of Heterogeneous Sandstone Reservoirs, Springer, 2017, http://dx.doi.org/10.1007/978-3-662-53287-4.
[12] M. Zandvliet, M. Handels, G. Van Essen, D. Brouwer, J.-D. Jansen, Adjoint-based well-placement optimization under production constraints, Spe J. 13 (04) (2008) 392–399.
[13] T. Roberts-Ashby, B. Ashby, A method for examining the geospatial distribution of CO2 storage resources applied to the Pre-Punta Gorda Composite and Dollar Bay reservoirs of the South Florida Basin, USA, Mar. Pet. Geol. 77 (2016) 141–159, http://dx.doi.org/10.1016/j.marpetgeo.2016.06.010.
[14] C.J. Willems, A. Vondrak, H.F. Mijnlieff, M.E. Donselaar, B.M. Van Kempen, Geology of the Upper Jurassic to Lower Cretaceous geothermal aquifers in the West Netherlands Basin - An overview, Geol. Mijnbouw/Neth. J. Geosci. 99 (2020) 1–13, http://dx.doi.org/10.1017/njg.2020.1.
[15] M. Major, A. Daniilidis, T.M. Hansen, M. Khait, D. Voskov, Influence of process-based, stochastic and deterministic methods for representing heterogeneity in fluvial geothermal systems, Geothermics 109 (2023) 102651, http://dx.doi.org/10.1016/j.geothermics.2023.102651.
[16] Y. Wang, D. Voskov, A. Daniilidis, M. Khait, S. Saeid, D. Bruhn, Uncertainty quantification in a heterogeneous fluvial sandstone reservoir using GPU-based Monte Carlo simulation, Geothermics 114 (2023) 102773, http://dx.doi.org/10.1016/j.geothermics.2023.102773.
[17] O. Badru, C. Kabir, Well placement optimization in field development, in: Paper SPE 8419 Presented at the SPE Annual Technical Conference and Exhibition, Denver, Colorado, 2003.
[18] F. Forouzanfar, G. Li, A.C. Reynolds, A two-stage well placement optimization method based on adjoint gradient, in: SPE Annual Technical Conference and Exhibition, Society of Petroleum Engineers, 2010, p. 1.
[19] O. Leeuwenburgh, P. Egberts, O. Abbink, Ensemble methods for reservoir life-cycle optimization and well placement, in: Paper SPE 136916 for Presentation At the 2010 SPE/DGS Annual Technical Symposium and Exhibition Held in Al_Khobar, Saudi Arabia 4–7 April 2010, 2010, p. 1.
[20] K. Zhang, H. Zhang, L. Zhang, P. Li, X. Zhang, J. Yao, A new method for the construction and optimization of quadrangular adaptive well pattern, Comput. Geosci. 21 (3) (2017) 499–518, http://dx.doi.org/10.1007/s10596-017-9626-3.
[21] E. Ansari, R. Hughes, C.D. White, Well placement optimization for maximum energy recovery from hot saline aquifers, in: 39th Workshop on Geothermal Reservoir Engineering, SGP-TR-202, Stanford University, Stanford, 2014, p. 1.
[22] M. Chen, A.F. Tompson, R.J. Mellors, O. Abdalla, An efficient optimization of well placement and control for a geothermal prospect under geological uncertainty, Appl. Energy 137 (2015) 352–363, http://dx.doi.org/10.1016/j.apenergy.2014.10.036.
[23] Y. Kong, Z. Pang, H. Shao, O. Kolditz, Optimization of well-doublet placement in geothermal reservoirs using numerical simulation and economic analysis, Environ. Earth Sci. 76 (2017) 1–7, http://dx.doi.org/10.1007/s12665-017-6404-4.
[24] J.E. Onwunalu, L.J. Durlofsky, Development and application of a new well pattern optimization algorithm for optimizing large-scale field development, Proc. SPE Annu. Tech. Conf. Exhib. 3 (2009) 1926–1943, http://dx.doi.org/10.2118/124364-ms.
[25] S. Zhang, Z. Jiang, S. Zhang, Q. Zhang, G. Feng, Well placement optimization for large-scale geothermal energy exploitation considering nature hydro-thermal processes in the Gonghe Basin, China, J. Clean. Prod. 317 (2021) 128391, http://dx.doi.org/10.1016/j.jclepro.2021.128391.
[26] Y. Nasir, O. Volkov, L.J. Durlofsky, A two-stage optimization strategy for large-scale oil field development, Optim. Eng. (2022) http://dx.doi.org/10.1007/s11081-020-09591-y.
[27] K. Zhang, Y. Chen, L. Zhang, J. Yao, W. Ni, H. Wu, H. Zhao, J. Lee, Well pattern optimization using NEWUOA algorithm, J. Pet. Sci. Eng. 134 (2015) 257–272, http://dx.doi.org/10.1016/j.petrol.2015.02.017.
[28] C. Zaal, A. Daniilidis, F.C. Vossepoel, Economic and fault stability analysis of geothermal field development in direct-use hydrothermal reservoirs, Geotherm. Energy 9 (1) (2021) 1–26, http://dx.doi.org/10.1186/s40517-021-00193-0.
[29] Y. Wang, D. Voskov, M. Khait, S. Saeid, D. Bruhn, Influential factors on the development of a low-enthalpy geothermal reservoir: A sensitivity study of a realistic field, Renew. Energy 179 (2021) 641–651, http://dx.doi.org/10.1016/j.renene.2021.07.017.
[30] C.J. Willems, H.M. Nick, T. Goense, D.F. Bruhn, The impact of reduction of doublet well spacing on the Net Present Value and the life time of fluvial Hot Sedimentary Aquifer doublets, Geothermics 68 (2017) 54–66, http://dx.doi.org/10.1016/j.geothermics.2017.02.008.
[31] M. Khait, Delft Advanced Research Terra Simulator: General Purpose Reservoir Simulator with Operator-Based Linearization, Delft University of Technology, 2019, URL https://repository.tudelft.nl/islandora/object/uuid:5f0f9b80-a7d6-488d-9bd2-d68b9d7b4b87?collection=research.
[32] D. Voskov, Delft advanced research terra simulator, 2021, URL https://darts.citg.tudelft.nl/. (Accessed 31 October 2021).
[33] M. Khait, D.V. Voskov, Operator-based linearization for general purpose reservoir simulation, J. Pet. Sci. Eng. 157 (July 2017) (2017) 990–998, http://dx.doi.org/10.1016/j.petrol.2017.08.009.
[34] M. Khait, D. Voskov, Adaptive parameterization for solving of thermal/compositional nonlinear flow and transport with buoyancy, SPE J. 23 (02) (2018) 522–534, http://dx.doi.org/10.2118/182685-PA.
[35] M. Khait, D. Voskov, Operator-based linearization for efficient modeling of geothermal processes, Geothermics 74 (2018) 7–18, http://dx.doi.org/10.1016/j.geothermics.2018.01.012.
[36] Y. Wang, M. Khait, D. Voskov, S. Saeid, D.F. Bruhn, Benchmark test and sensitivity analysis for Geothermal Applications in the Netherlands, Proc. 44th Work. Geotherm. Reserv. Eng. 2 (2019) 1–11, URL https://pangea.stanford.edu/ERE/db/GeoConf/papers/SGW/2019/Wang6.pdf.
[37] Y. Wang, D. Voskov, M. Khait, D. Bruhn, An efficient numerical simulator for geothermal simulation: A benchmark study, Appl. Energy 264 (October 2019) (2020) http://dx.doi.org/10.1016/j.apenergy.2020.114693.
[38] M.J. O'Sullivan, K. Pruess, M.J. Lippmann, State of the art geothermal reservoir simulation, Geothermics 30 (4) (2001) 395–429, http://dx.doi.org/10.1016/S0375-6505(01)00005-0.
[39] A. Daniilidis, B. Alpsoy, R. Herber, Impact of technical and economic uncertainties on the economic performance of a deep geothermal heat system, Renew. Energy 114 (2017) 805–816, http://dx.doi.org/10.1016/j.renene.2017.07.090.
[40] A. Daniilidis, H.M. Nick, D.F. Bruhn, Interdependencies between physical, design and operational parameters for direct use geothermal heat in faulted hydrothermal reservoirs, Geothermics 86 (September 2019) (2020) 101806, http://dx.doi.org/10.1016/j.geothermics.2020.101806.
[41] TNO, Economic model (thermogis), 2019.
[42] C. Statline, 2021. link (Accessed October 2021).
[43] S.C. Endres, C. Sandrock, W.W. Focke, A simplicial homology algorithm for Lipschitz optimization, J. Global Optim. 72 (2) (2018) 181–217, http://dx.doi.org/10.1007/s10898-018-0645-y.
[44] S. Endres, Simplicial homology global optimisation - github, 2019, URL https://stefan-endres.github.io/shgo/.
[45] S. Endres, C. Sandrock, Shgo documentation, 2021.
[46] S.K. Garg, J. Combs, A reformulation of USGS volumetric "heat in place" resource estimation method, Geothermics 55 (2015) 150–158, http://dx.doi.org/10.1016/j.geothermics.2015.02.004.
[47] A. Daniilidis, M. Khait, S. Saeid, D. Bruhn, D. Voskov, A high performance framework for the optimization of geothermal systems, comparing energy production and economic output, in: Proceedings World Geothermal Congress. 2020a, 2020, pp. 491–515.
[48] P. Vardon, H. Abels, A. Barnhoorn, A. Daniilidis, D. Bruhn, G. Drijkoningen, K. Elliott, B. van Esser, S. Laumann, P. van Paassen, et al., A research and energy production geothermal project on the TU delft campus: project implementation and initial data collection, in: 49th Stanford Geothermal Workshop, 2024.
[49] J.E. Onwunalu, L.J. Durlofsky, Application of a particle swarm optimization algorithm for determining optimum well location and type, Comput. Geosci. 14 (1) (2010) 183–198, http://dx.doi.org/10.1007/s10596-009-9142-1.
[50] M.L. Litvak, P.F. Angert, Field development optimization applied to giant oil fields, in: SPE Reservoir Simulation Conference, SPE, 2009, pp. SPE–118840.